ISSN 2616-5767 Vol.7, Issue 2: 130-137, DOI: 10.25236/AJETS.2024.070219

A Piezoelectric Wind Energy Harvester for Low Speed Air-flows

Bo Niu

School of Mechatronics Engineering, Henan University of Science and Technology, Luoyang 471003, Henan, China
zsnb345@gmail.com

Abstract: *This paper reports a detailed modelling, parameter effect and developmental experimental investigation of a piezoelectric wind energy harvester with interaction between vortex-induced vibration and galloping for the low speed air flows. The influence factors such as mechanical damping, mass, and the cross section dimension on the interaction are explored in turn. Guidance based on the above discussion, a prototype is fabricated and measured successfully. The experimental results agreed well with the theoretical predictions. The proposed model is an effective tool to develop the interactive piezoelectric wind energy harvester working in low wind speed regions.*

Keywords: *Energy harvesting, Modelling, Vortex-induced vibration, Galloping, Piezoelectricity*

1. Introduction

Piezoelectric wind energy harvesters (PWEHs) based-on wind-induced vibration can be miniaturized by micromachining and attract much attention recently[1]. PWEHs can produce usable electrical energy only when the wind speed is higher than the critical speed. In the response to this, the velocities of natural air-flows are generally low. So high electrical output with low critical wind speed of PWEHs is the constant and unsophisticated aim for researchers to widen the applications naturally[2]. As the responses of vortex-induced vibration (VIV) are much lower than other types of wind-induced vibration such as galloping, flutter, and wake galloping, PWEHs based on galloping or flutter are preferred[3-5]. But unfortunately, the critical wind speed of PWEHs based VIV is usually the lowest because of its mechanism. In addition, one of the other main concerns of researchers is to investigate the influence of different bluff body shapes on the performance of PWEHs[6,7]. Recently, He et al. experimentally found that, though the electrical output produced by VIV is small, VIV can be used to greatly enlarge the output power at low wind speeds by the interaction with galloping. This provides researchers with a new idea that the interaction between VIV and galloping to PWEHs can effectively reduce the critical wind speed and improve the performance at the same time.

The quasi steady state model of galloping vibration was combined with the VIV model of Tamura and Matsui to simulate the mechanical response of a rectangular blunt body with interaction between VIV and galloping vibration [8-10]. Some researchers have been systematically and deeply studied the mechanical model of the interaction through theory and experiment[11-13]. To expend the model to piezoelectric PWEHs, piezoelectric effects need to be introduced into the equation of motion and an electrical equation should be developed to simulate the electrical responses. This article first derives the lumped parameter electromechanical and pneumatic models of interactive PWEH, and successfully applies them to the development of interactive PWEH. The influence factors such as mechanical damping, mass, and the cross section dimension on the interaction are also explored in turn. Based on the above discussion, a prototype of PWEH with interaction was fabricated and experiment successfully. The experimental results agreed well with the theoretical predictions. The proposed model is an effective tool to develop the interactive PWEHs working in low wind speed regions.

2. Model Description

According to the quasi-steady theory, the bluff body placed in air flow will be acted by an asymmetric aerodynamic force on its sides and then subjected a transverse aeroelastic instability. So, a piezoelectric composite cantilever beam with one end fixed and another end attached to a bluff body will be experienced a similar unstable vibration. The load resistance gains sinusoidal electrical output through

ISSN 2616-5767 Vol.7, Issue 2: 130-137, DOI: 10.25236/AJETS.2024.070219

the electrodes which extracted from the piezoelectric beam, as shown in the schematic presented in Figure 1. The cantilever was fabricated by using a layer of ultraviolet (UV) –curing adhesive to attach a polyvinylidene fluoride (PVDF) film and a polyethylene terephthalate (PET) substrate with the same length and width.

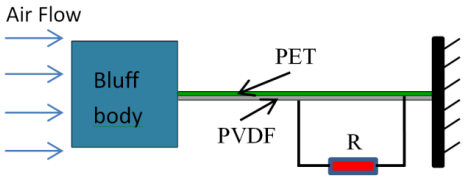

Figure 1: Schematic of the piezoelectric PWEH.

Considering the Euler-Bernoulli beam theory and the Gauss law, the governing equations of motion and electric of the proposed piezoelectric PWEH can be expressed as follows[7]:

$$M\ddot{y}(t) + C\dot{y}(t) + Ky(t) + \Theta V(t) = F_y(t) \tag{1}$$

$$C_p\dot{V}(t) + \frac{V(t)}{R} = \Theta\dot{y}(t) \tag{2}$$

Where $y(t)$ is the displacement amplitude of the square cross-section bluff body. M, C, K are the corresponding equivalent mass, damping and stiffness of system, respectively. The system capacitance and the piezoelectric coupling term are given by C_p and Θ. The fluid force is given by $F_y(t) = F_{VIV}(t) + F_{galloping}(t)$ which come from VIV and galloping, respectively.

Many optimized van der Bohr oscillator models can be used to capture the characteristics of the self limiting response of VIV, and these optimized models have achieved good applications in practice. [9,14]. According to the model proposed by Tamura and Matsui in 1979, the fluid force of VIV is directly related to the angle displacement of wake oscillator as follows:

$$\ddot{\alpha} + 2\zeta\omega_{VIV}\left[\left(\frac{2f}{C_{L0}}\right)\alpha^2 - 1\right]\dot{\alpha} + \omega_{VIV}^2\left(\alpha + \frac{\dot{y}}{u}\right) = -\frac{\ddot{y}}{(0.5+l^*)D} \tag{3}$$

Where the constant $f = 1.16$ is estimated by the relationship observed experimentally between magnus effect lift and wake angular displacement for a bluff body. $l^* = \frac{L}{D} = 1.1$ is the ratio between the length of wake oscillator and the width of bluff body. ζ and ω_{VIV} are the damping ratio and natural frequency of wake oscillator. C_{L0} is the amplitude used to represent the fluctuating lift coefficient of a stationary blunt body.

In 1987, with combined quasi-steady theory and Tamura and Matsui model which adapted it to the case of a square from a circular cylinder, Tamura and Shimada obtained a mathematical model for the interaction between VIV and galloping[10]. The fluid force was finally expressed as:

$$F_y(t) = \frac{1}{2}\rho u^2 DL\left\{f\left(\alpha + \frac{\dot{y}}{u}\right) - \left[A_1\left(\frac{\dot{y}}{u}\right) + A_3\left(\frac{\dot{y}}{u}\right)^3 + A_5\left(\frac{\dot{y}}{u}\right)^5 + A_7\left(\frac{\dot{y}}{u}\right)^7\right]\right\} \tag{4}$$

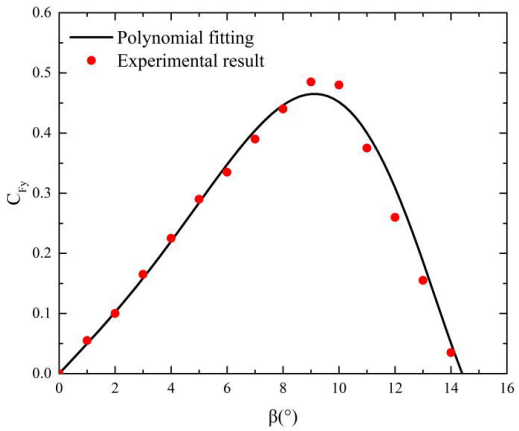

Figure 2: The aerodynamic force coefficient curves for experiment and fitting.

ISSN 2616-5767 Vol.7, Issue 2: 130-137, DOI: 10.25236/AJETS.2024.070219

Table 1: Coefficients of polynomial and determination.

Type	Turbulence intensity	A1	A3	A5	A7	R-Square
Turbulence flow	6.70%	2.83	90.75	-4248.3	30146.43	0.99252

The cross-section characteristics and turbulence intensity determine the composition of aerodynamic coefficients and then the fluid force forces of galloping. The aerodynamic force coefficient, using static measurement in turbulence flow on square cross-sections, was measured experimentally[15,16]. Fit the curve with a 7th order polynomial, as shown in Figure 2. The polynomial coefficients and determination coefficients are shown in Table 1.

Finally, the complete lumped-parameter electromechanical and aerodynamic model expression of proposed PWEH with interaction has been obtained by equation (1)~(4) with introducing the following definition:

$$Y = \frac{y}{D},\ \eta = \frac{C}{2\omega_n M},\ \omega_n = \frac{K}{M},\ n = \frac{\rho D^2 L}{2M},\ \upsilon = \frac{u}{u_{cr}} = \frac{\omega_{VIV}}{\omega_n},$$

$$\tau = \omega_n t,\ m^* = 1/(1+l^*),\ S^* = 2\pi S_t = \sqrt{\pi/h^*(1+l^*)}$$

Those equations are convenient to rewrite as follows:

$$\ddot{Y} + \left[2\eta + n(f - A_1)\frac{\upsilon}{S^*} - \sum_{i=2}^{N} nA_i \left(\frac{S^*}{\upsilon}\right)^{i-2} \dot{Y}^{i-1}\right]\dot{Y} + Y + \frac{\Theta}{M\omega_n^2 D} V = -fn\vartheta\left(\frac{\upsilon}{S^*}\right)^2 \tag{5}$$

$$\ddot{\alpha} + 2\zeta\upsilon\left[\left(\frac{2f}{C_{L0}}\right)\alpha^2 - 1\right]\dot{\alpha} + \upsilon^2\alpha = -m^*\ddot{Y} - \upsilon S^*\dot{Y} \tag{6}$$

$$\frac{V}{\omega_n DR} + \frac{C_p}{D}\dot{V} = \Theta\dot{Y} \tag{7}$$

3. Influence Factors on the Interaction

3.1. Parameter Identification

Considering the following investigation of influence factors such as mechanical damping, mass, and the cross section dimension on the interaction, the parameters of the prototype need to be identified by experiment. A prototype of the interactive piezoelectric PWEH device was fabricated, as shown in Figure 3, and tested in a small wind tunnel which the maximum wind speed can be reached 14m/s through a frequency modulation motor. The bluff body was made from low density polystyrene foam for prototype, with a square cross section. The cantilever was fabricated by using the ultraviolet (UV) -curing to make a same polyvinylidene fluoride (PVDF) film and a polyethylene terephthalate (PET) substrate with the same length and width, respectively. The total equivalent mass is 0.0164. The prototype fixed rigidly onto a steel cylinder in the working section of wind tunnel. The wind velocity and the output voltage of the harvester were monitored by an anemometer and oscillography, respectively. The harvester's natural frequency (means the short circuit natural frequency) was measured in the short circuit condition and was about 212.88 rad/s. The system capacitance C_P was 95.9 pF which measured by LCR meter. The optimal load resistance can be approximated by $R_L = 1/\omega_n C_p$ and was calculated as 48.73 MΩ. The mechanical damping ratio of prototype was calculated to be approximately 1.2%, by using the logarithmic decrement method. The detailed parameters of the prototype is given in Table 2.

According to the prediction of model, the prototype we fabricated with above properties should be belong to the interactive piezoelectric PWEH. For experimental data of prototype, the electrical output was obtained with a load resistance of 10 MΩ, and there was only one wind speed region with high electrical output so that the VIV and galloping cannot be distinguished, as shown in Figure 4. The experimental actual onset speed was between 1.2 to 1.3 m/s. The RMS voltage increased from 0.05 V to 30.00 V when the wind speed increased from 1.2 to 5 m/s, and the electrical response nearly linear increased.

ISSN 2616-5767 Vol.7, Issue 2: 130-137, DOI: 10.25236/AJETS.2024.070219

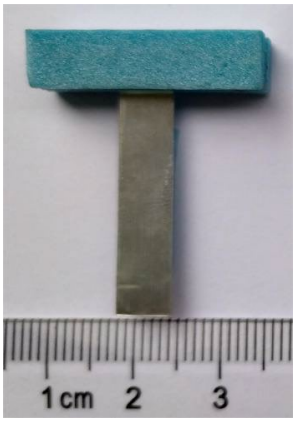

Figure 3: Photo of an interactive PWEH prototype.

Table 2: Properties of the proposed piezoelectric PWEH prototype.

Parameter	Symbol	Value
Characteristic dimension (mm)	B×D×L	8×8×25
PVDF Young's modulus (GPa)	Yp	2.75
PET Young's modulus (GPa)	Ys	3.40
Strain coefficient of piezoelectric layer (Pc/N)	d31	-24
Permittivity component at constant strain (pF/m)	ε33	115.1
Equivalent mass (g)	M	0.0164
Natural frequency (rad)	ωn	212.88
Strouhal number	St	0.13
Mass ratio	n	0.003
Mechanical damping ratio	η	0.012
Steady lift coefficient	CL0	0.2
Constant related to the Mangus effect	f	1.16
	ζ	0.0257
Constant related to the St number	S*	0.8168
Constant related to acceleration of cylinder	m*	0.3823
Electromechanical coupling coefficient	Θ	1.52E-06
Capacitance (pF)	Cp	95.9
Load resistance (MΩ)	R	48.73
Air density (kg/m^3)	ρ	1.205

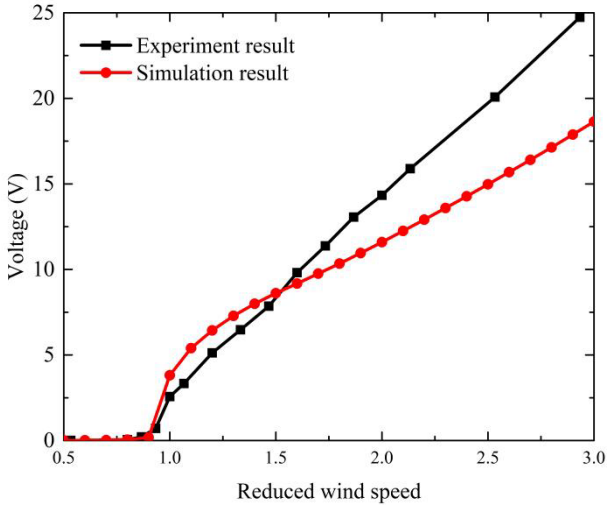

Figure 4: Experiment and simulation voltage results versus reduced wind speed(υ).

Introduced the value of all parameter above into the proposed model, the simulate output was calculated finally with reduced wind speed, as shown in Figure 4. The model we proposed successfully predicted the electrical response which had only one numerical wind speed region with high electrical output. The numerical critical wind speed of beginning oscillation is accord with the experimental but

ISSN 2616-5767 Vol.7, Issue 2: 130-137, DOI: 10.25236/AJETS.2024.070219

the slope of numerical curve is underestimated in the all wind speed region. The reason for the overestimation may came from the Young's modulus of UV curing and the constant f. This first data may be inaccurate because the manufacturer does not provide, the second one was determined by experimental study for the circular cylinder. Tamura and Shimada applied to the square section with no adjustment for TS-model[9,10].

According to our preliminary calculation studies, the constant f played an important role in reproducing the slope of the growing branch of the response. When the value around 3.48 (three times the nominal value) was introduced, the overestimation had been disappeared which made the final numerical curve highly consistent with the experiment result. But we did not do that and the unembellished numerical result was displayed in finally. Because of no considering nonlinearity of proposed model, the prediction of response in nonlinear increase region was failed. It is very normal that study on nonlinear distributed parameter model is the focus of the next stage. The comparison of experiment and numerical results shown that the model has the highly applicability in predicting the electrical response of the VIV-galloping PWEHs with interaction not only in quality but also in quantity in linear increase region.

3.2. Influence of Factor of the Damping Ratio

The impact of the damping ratio on the behavior of interaction and the performance of the prototype is simulated successfully, as shown in Figure 5. A complete process from separation to the interaction between VIV and galloping vibration is display with decreasing damping ratio. There are two independent wind speed zones with relatively high electrical output, belonging to VIV and galloping vibration respectively, while damping ratio is higher than 2.95%. It seems that the critical wind speed at which VIV begins to oscillate is immune to the damping ratio but the extent of oscillation is enlarged which means the one of maximum amplitude shifted to the right hand with decreasing damping ratio. According to the quasi-steady theory, the galloping critical wind speed, $u_g = \frac{8\pi M\eta f_n}{\rho LDA_1}$, is impacted linearly by damping ratio that as the same to the simulate results.

According to the simulate results, there is a sudden transform from separation to interaction when the damping ratio is between 2.9% to 2.95%. For the two interactive cases, the galloping critical wind speed is still higher than the critical wind speed of VIV. So, the critical wind speed of beginning oscillation is also means the one of VIV and immune to the damping ratio. The effect of the damping ratio on the performance of the region of VIV and galloping is consistency that the performance decreasing linearly with the increasing damping ratio.

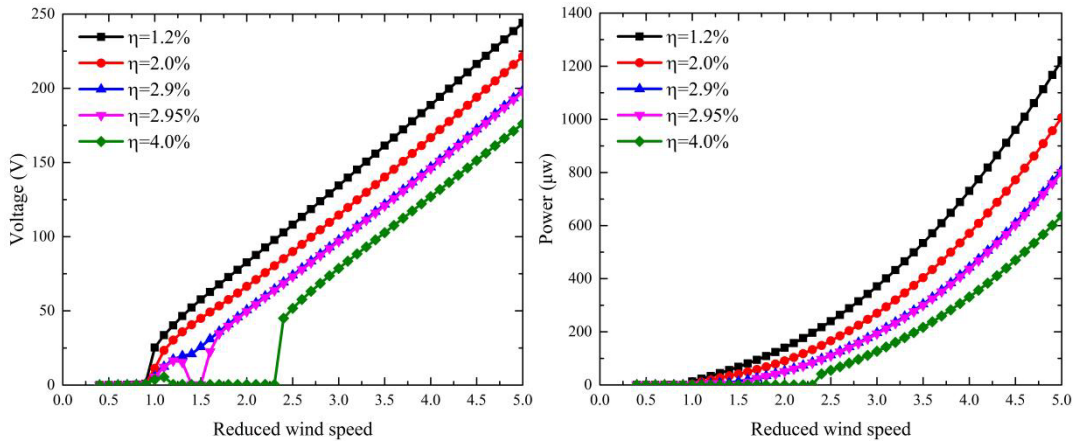

Figure 5: Voltage and power versus reduced wind speed(υ) with different damping ratios.

3.3. Influence of Factor of the Dimension of Cross-section

Four different dimensions are introduced in to the model, namely, 4mm, 5mm, 6mm, 7mm, and 8mm. An increase in the cross-section dimension is accompanied by the transformation from separation to interaction and an increase in the output, as shown in Figure 6. Comparison of the effect of damping ratio, the behavior of interaction is significant sensitive to the dimension of cross-section. This conclusion is validated not only in previous study but also in subsequent new experiments (not appear in this paper). In addition, comparison the simulate results between 4mm and 5mm cases, the galloping critical wind

ISSN 2616-5767 Vol.7, Issue 2: 130-137, DOI: 10.25236/AJETS.2024.070219

speed of 4mm case is almost two times the one of 5mm case, showing a strong influence of cross-section dimension on the galloping critical wind speed. This is not in line with the prediction of galloping critical wind speed by quasi-steady theory, $u_g = \frac{8\pi M\eta f_n}{\rho LDA_1}$, which should be linearly with cross-section dimension. It is confirmed that the fluid force of VIV runs through the whole wind speed region which can be validated from the parameter n in the equation (5). As for the performance, it is conformed to expectation that larger cross-section dimension will be subjected larger fluid force according to the equation (4), which cause to the larger displacement and the higher output.

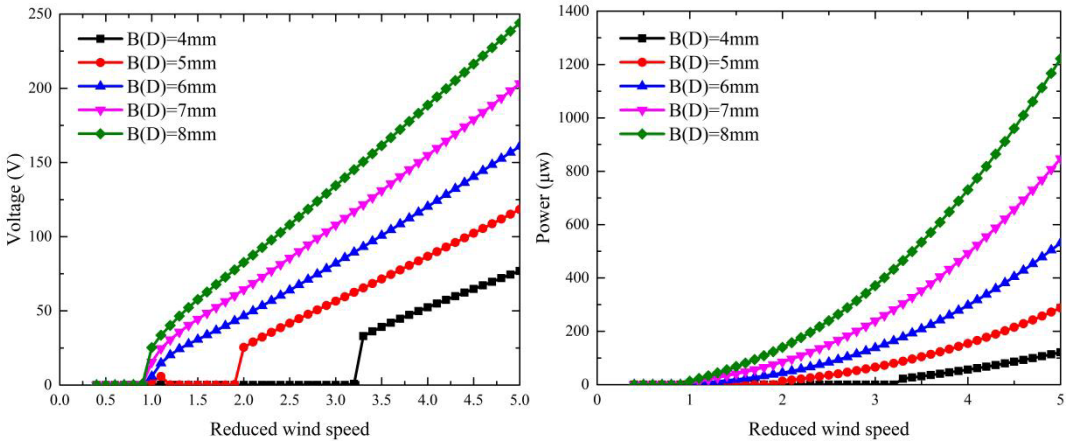

Figure 6: Voltage and power versus reduced wind speed(υ) with different cross sections dimension.

4. Numerical Results of Different Model

As pointed out in the introduction, a mathematical motion model of square cross-section bluff body for the interreaction among VIV and galloping was raised by Tamura and Shimada in 1987, who combined quasi-steady theory and TM-model which adjusting it to a square from a circular cylinder. The numerical results with only one type model is also investigated for the interactive case. By substituting $A_1 = A_3 = A_5 = A_7 = 0$ into equation (5), the lumped-parameter electromechanical and aerodynamic model of VIV of PWEHs can be obtained:

$$\ddot{Y} + \left[2\eta + n(f + C_D)\frac{\upsilon}{S^*}\right]\dot{Y} + Y + \frac{\Theta}{M\omega_n^2 D}V = -fn\vartheta\left(\frac{\upsilon}{S^*}\right)^2 \tag{8}$$

$$\ddot{\alpha} + 2\zeta\upsilon\left[\left(\frac{2f}{C_{L0}}\right)\alpha^2 - 1\right]\dot{\alpha} + \upsilon^2\alpha = -m^*\ddot{Y} - \upsilon S^*\dot{Y} \tag{9}$$

$$\frac{V}{\omega_n DR} + \frac{C_p}{D}\dot{V} = \Theta\dot{Y} \tag{10}$$

Where C_D is the drag coefficient which is equal to 1.88. It should be mentioned that because C_D has been include in coefficient A_1, it is not appear to the above model we proposed alone.

In addition, by substituting $\alpha = 0$, the fluid force of VIV can be eliminated and then the lumped-parameter model of galloping which same to the previous study can be given as follow:

$$\ddot{Y} + \left[2\eta - nA_1\frac{\upsilon}{S^*} - \sum_{i=2}^{N} nA_i\left(\frac{S^*}{\upsilon}\right)^{i-2}\dot{Y}^{i-1}\right]\dot{Y} + Y + \frac{\Theta}{M\omega_n^2 D}V = 0 \tag{11}$$

$$\frac{V}{\omega_n DR} + \frac{C_p}{D}\dot{V} = \Theta\dot{Y} \tag{12}$$

Figure 7 shows the numerical output of three different models with increasing wind speed. According to the results, there is an interesting phenomenon that the outputs of VIV and galloping model alone are all lower than the one of interactive model. This means that when the critical wind speed for galloping is low enough, the interaction between VIV and galloping is mutually reinforcing, which means that the interaction between VIV and galloping will be enhanced.

ISSN 2616-5767 Vol.7, Issue 2: 130-137, DOI: 10.25236/AJETS.2024.070219

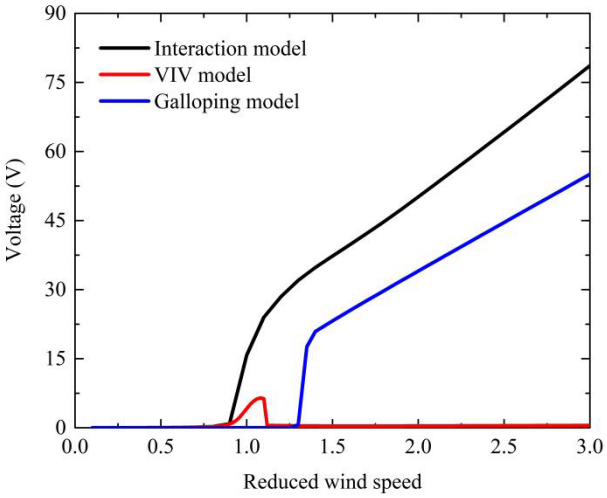

Figure 7: Simulation results for various models.

5. Conclusions

This article mainly focuses on the detailed lumped parameter electromechanical modeling parameter effects and development experimental research of piezoelectric PWEH with vortex induced vibration and galloping interaction in low-speed airflow. The influence factors on the interaction are explored in turn. Compared with the effect of damping ratio, the behavior of interaction is significant sensitive to the dimension of cross-section on this scale. The proposed interactive model can be convenient reduced into the lumped-parameter model of the piezoelectric PWEH based on VIV or galloping only. The numerical output of three different models with increasing wind speed has been exhibited. It indicated that the effects of VIV and galloping are mutually reinforcing once the interaction germinated. Guidance based on the above conclusion, a prototype of PWEH with interaction is fabricated and measured successfully. The experimental results agreed well with the theoretical predictions. The proposed model is an effective tool to develop the interactive PWEHs working in low wind speed regions.

References

[1] A. Erturk, W. G. Vieira, C. De Marqui and D. J. Inman. On the energy harvesting potential of piezoaeroelastic system[J]. Applied Physics Letters. 2010, 96: 184103.
[2] X. F. He, Z. G. Shang and S. L. Jiang. Discrepancy between galloping theory and experiment on a MEMS piezoelectric wind energy harvester[C]. The 19th International Conference on Solid-State Sensors, Actuators and Microsystems, Kaohsiung, Taiwan, 2017.
[3] A. Bibo, M. F. Daqaq. On the optimal performance and universal design curves of galloping energy harvesters[J]. Applied Physics Letters, 2014, 104: 023901.
[4] R. Naseer, H. L. Dai, A. Abdelkefi and L. Wang. Piezomagnetoelastic energy harvesting from vortex-induced vibrations using monostable characteristics[J]. Applied Energy, 2017, 203: 142-53.
[5] H. L. Dai, A. Abdelkefi, Y. Yang and L. Wang. Orientation of bluff body for designing efficient energy harvesters from vortex-induced vibrations[J]. Applied Physics Letters, 2016, 108: 053902.
[6] G. Hu, K. T. Tse, M. Wei, R. Naseer, A. Abdelkefi and K. C. S. Kwok. Experimental investigation on the efficiency of circular cylinder-based wind energy harvester with different rod-shaped attachments[J]. Applied energy, 2018, 226: 682-689.
[7] Y. W. Yang, L. Y. Zhao and L. H. Tang. Comparative study of tip cross-sections for efficient galloping energy harvesting[J]. Applied Physics Letters, 2013, 102(6): 064105.
[8] J. D. Smith. An experimental study of the aeroelastic instability of rectangular cylinders[D]. Ph.D. Dissertation, UBC, Vancouver, Canada; 1962.
[9] Y. Tamura and G. Matsui. Wake-oscillator model of vortex-induced oscillation of circular cylinder[C]. The 5st International Conference on Wind Engineering, Fort Collins, Colorado, USA, 1979.
[10] Y. Tamura and K. Shimada. A mathematical model for the transverse oscillations of square cylinders[C]. The 1st International Conference on Flow Induced Vibrations, Bowness on Windermere, England, 1987.
[11] C. Mannini, A. M. Marra, T. Massai and G. Bartoli. Interference of vortex-induced vibration and

ISSN 2616-5767 Vol.7, Issue 2: 130-137, DOI: 10.25236/AJETS.2024.070219

transverse galloping for a rectangular cylinder[J]. Journal of Fluids Structures, 2016, 66: 403-23.
[12] H. W. Niu, S. Zhou, Z. Q. Chen and X. G. Hua. An empirical model for amplitude prediction on VIV-galloping instability of rectangular cylinders[J]. Wind and Structures, 2015:21(1), 85-103.
[13] C. Mannini, T. Massai and A. M. Marra. Modeling the interference of vortex-induced vibration and galloping for a slender rectangular prism[J]. Journal of Sound Vibration, 2018, 419: 493-509.
[14] M. L. Facchinetti, E. D. Langre and F. Biolley. Coupling of structure and wake oscillators in vortex-induced vibrations[J]. Journal of Fluids and Structures, 2004, 19: 123-40.
[15] A. Laneville. Effects of turbulence on wind induced vibrations of bluff cylinders[D]. Ph.D. Dissertation, UBC, Vancouver, Canada; 1973.
[16] A. Barrero-Gil. A. Sanz-Andrés and G. Alonso. Hysteresis in transverse galloping: the role of the inflection points[J]. Journal of Fluids and Structures, 2009, 25: 1007-20.